A Comparative Study on Voxel Classification Methods for Atlas based Segmentation of Brain Structures from 3D MRI Images

Gaetan Galisot[1], Thierry Brouard[1], Jean-Yves Ramel[1] and Elodie Chaillou[2]

[1]*LIFAT Tours, Université de Tours, 64 avenue Jean Portalis, 37000, Tours, France*
[2]*PRC, INRA, CNRS, IFCE, Université de Tours, 37380, Nouzilly, France*

Keywords: 3D Image Segmentation, Local Atlas, Voxels Classification.

Abstract: Automatic or interactive segmentation tools for 3D medical images have been developed to help the clinicians. Atlas-based methods are one of the most usual techniques to localized anatomical structures. They have shown to be efficient with various types of medical images and various types of organs. However, a registration step is needed to perform an atlas-based segmentation which can be very time consuming. Local atlases coupled with spatial relationships have been proposed to solve this issue. Local atlases are defined on a sub-part of the image enabling a fast registration step. The positioning of these local atlases on the whole image can be done automatically with learned spatial relationships or interactively by a user when the automatic positioning is not well performed. In this article, different classification methods possibly included in local atlases segmentation methods are compared. Human brain and sheep brain MRI images have been used as databases for the experiments. Depending on the choice of the method, segmentation quality and computation time are very different. Graph-cut or CNN segmentation methods have shown to be more suitable for interactive segmentation because of their low computation time. Multi-atlas based methods like local weighted majority voting are more suitable for automatic process.

1 INTRODUCTION

Manual annotation of anatomical structures in 3D medical images is a laborious task for clinicians and biologists. Manual segmentation is still performed slide by slide and can be very time consuming. Development of tools helping to study the different types of medical images is important. That is why, a lot of automatic methods have been proposed to provide segmentation on various type of anatomical structures and organs.

Atlas-based segmentation methods are ones of the most usual types of techniques used for medical images (Cabezas et al., 2011). A training database, composed of several 3D medical images and the labeled maps associated, is used to build an atlas of an organ. Then, the segmentation is performed in two steps; the atlas is first registered to the image that the user wants to segment, then a segmentation (voxel classification) method is applied, merging the information coming from the image and the atlas. Different ways exist to model a priori information. In particular probabilistic atlas, multi-atlas or statistical shape model are often used. In this work, we focus on the volume atlases.

One of the usual drawbacks is the computation time of the atlas-based methods. The atlas is usually defined on the whole organ. Then, the segmentation needs at least one non-linear registration step which is time consuming when the size or the resolution of the image is important. We can also note that the atlas-based segmentation are usually fully automatic and does not let the opportunity to the user to drive the segmentation process.

In order to obtain more interactive and faster partial segmentations, local atlases have been proposed in (Galisot et al., 2017). These atlases are built on a small part of the image corresponding to the bounding box of each region. Each anatomical structure is described by its own template. Because of the small size of the sub-image, the registration step is performed in a faster way. To do the registration, local atlases must be positioned (superposed) inside the whole image to be segmented according to the known spatial relationships between regions that have to be learned from the training dataset. The user has also the possibility to help the system by re-positioning the borders of the bounding box of the local atlas inside the whole image if necessary. By this interaction, the system

can be driven or optimized by the user if the segmentation result is not satisfactory. The local approach provides significant advantages compared to the global one. First the information about the variability of the shape is separated from the information about the positioning positioning. Of course the computation time for a local registration significantly reduced compared to a global registration. But, the local segmentation brings also questions about the impact of the local positioning and registration on the result provided by voxel classification step. It is important to study how the different possible voxel classification methods usually used in global atlas-based approach are able to deal with a local, incremental and interactive segmentation way.

Section 2 reminds how the local atlases and spatial relationships are built and used during a segmentation. Section 3 presents six methods of voxels classification are studied in this paper; hidden Markov random field, simple voting method, local weighted voting method, joint label fusion method, Graph-cut and CNN. In section 4, two databases of brain images are presented and experiments comparing the different methods are described. Results are discussed in Section 5, explaining which classification method is the most suitable based on the experiment results.

2 LOCAL ATLAS SEGMENTATION

An atlas is an a priori information which needs a classification method to provide a final segmentation. A various type of classifications have been described in literature using either probabilistic or multi-atlas information. Multi-atlas based segmentation has provided great results on the segmentation of brain images (Iglesias and Sabuncu, 2015). A part or the totality of the training images are registered to the image to be segment. Voxels classification for multi-atlas have been mainly based on majority voting method (Rohlfing et al., 2004; Klein et al., 2005) and the most frequent label provided by the training labeled maps is chosen. Probabilistic atlases encode the probability to observe an anatomical structure in a certain position (Shattuck et al., 2008; Nitzsche et al., 2015). The training images of a population are merged by registering all the training images to the same space. They have been combined with a Gaussian mixture model (Ashburner and Friston, 2005), hidden Markov random field (Scherrer et al., 2009) or graph-cut methods (Dangi et al., 2017).

The work described in (Galisot et al., 2017), proposes to use different atlases defined locally to loca-

lize anatomical structures. Each anatomical structure is described by its own atlas. Within this method, during the learning step, the local atlases and the spatial relationships between them should be learned from a database. Thereafter, this learned model can be used to incrementally segment several anatomical structures in new images. The two following sections explain the construction of the model.

2.1 Local Atlas

A training database, composed of N couples of MRI and labeled images, is needed to construct the local atlases. Each region is learned independently from each other. Figure 1 describes the process of construction of the local atlases.

For each region r, the bounding boxes are detected in the labeled images and the volume inside is extracted and denoted by L_r. The corresponding volume in the MRI images is also extracted and denoted by B_r. In practice, a margin is added around the bounding boxes. This margin helps to decrease the influence of a wrong positioning and reduce abrupt frontiers in the probability maps. In the following, the bounding box term will refer to this extended bounding box.

At the end of this step, a local multi-atlas is already built. Each region r is described by N couples $\{B_r^a, L_r^a\}$ of images with $a = \{1, ..., N\}$. Two other steps are applied if a local probabilistic atlas is required. An intensity normalization is applied between the N MRI sub-images B_r. Then, the local probabilistic atlas for each structure is built incrementally. The couples $\{B_r^a, L_r^a\}$ of images are registered and the result is averaged providing a template T_r and probability map Pr_r.

2.2 Spatial Relationships

As we previously mention, the bounding boxes containing the local atlases can be positioned automatically by the system. Spatial relationships are learned between regions. These relationships allow to position each region compared to the others. In practice, the regions which are already located will provide information about the positioning of the next region to segment. Since these relations depends on the regions already located, the first region to segment can not be positioned automatically. The aim is also to, either help the user by proposing a position and limit the quantity of his interaction or perform an almost (only the initialization) fully automatic segmentation.

This spatial information is modeled as distances between the borders of each region. Relations are computed independently along the 3 common directi-
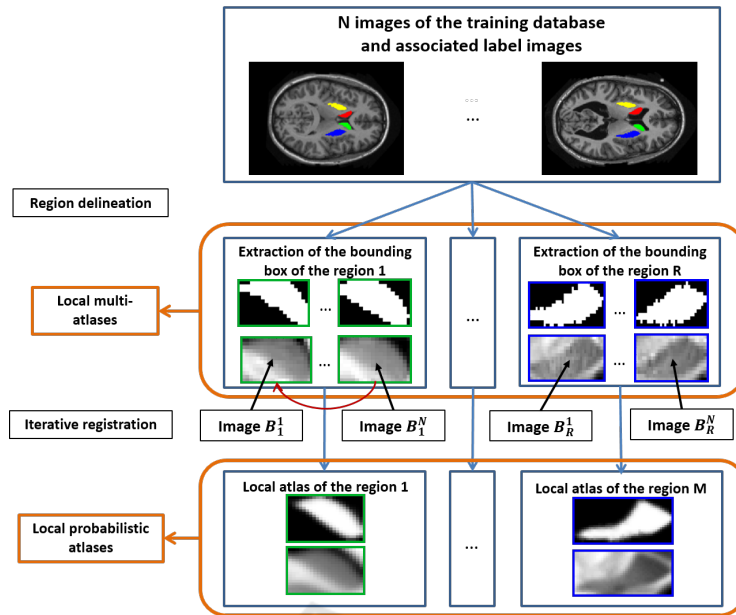
Figure 1: Process of construction of local atlases. Example with two anatomical structures (caudate nucleus, putamen) in human brain images (Galisot et al., 2017).

ons. In 3D, twelve distances are defined between two regions. In order to let the system independent from size or image resolution, distances are normalized compared to the size of the source region. Finally the minimum and the maximum of relative distances present in the training database is computed and stored.

During the segmentation, all the regions which are already segmented will provide information about the positioning of the next region r to segment. The positioning of a border of the bounding box is performed independently from the others. The different intervals of relative distances are selected and transformed in the absolute space of the new image. Then, the information coming from the different regions and different intervals are merged to obtain a final estimation of the position of the local atlas. The final position provides the volume Y_r which contains in the bounding box.

2.3 Incremental Segmentation

The segmentation using local atlases is performed incrementally and in an interactive way. The anatomical structures are localized sequentially. Contrary to a classical atlas, each region is described in its own space. Two different registrations are needed when two different regions are segmented. However, these registrations are performed very fast because of the small size of the different local atlases. Each atlas must be positioned inside the image to segment. This positioning can be done by the user. He or she must position the 6 borders of the bounding box of the region. This positioning can be also performed using spatial relationships (cf. Section 2.2). The volume inside the bounding box is denoted by Y_r. The local atlas of the region r is registered to Y_r.

If a probabilistic atlas is used, the transformation is determined by the registration of the template T_r to Y_r and the same transformation is then applied to the probability map Pr_r. If a multi-atlas method is used, N transformations are computed from B_r to the sub-image Y_r and the same transformation are applied to the labeled map L_r. Combination of this registered information with the MRI intensities in Y_r can be used as input information for the different classification processes discussed in the next section. The segmentation of a region is also definitive, meaning that the segmentation of a new region does not modify the result obtained for a previous region.

3 CLASSIFICATION METHOD

After the registration of the local atlas of the volume Y_r, a transformation τ is applied on the local probabilistic atlas $\{B_r, Pr_r\}$ (respectively a transformation τ_a on the local multi-atlas $\{B_r^a, L_r^a\}$). In the following, we will denoted by $\{B_r, Pr_r\}$ and $\{B_r^a, L_r^a\}$ instead of $\{B_r(\tau), Pr_r(\tau)\}$ and $\{B_r^a(\tau_a), L_r^a(\tau_a)\}$ respectively. A voxel classification must be used to obtain the final segmentation. The process is applied only inside the

sub-volume Y_r and not on the whole image.

A binary classification can be applied because only one region is sought in each sub-volume. A large amount of classification methods have been already coupled with atlas in the classical case. The following section describes these different segmentation methods we applied for the local approach case. In the following, Z_r denotes the binary segmentation of Y_r we want to segment.

3.1 Hidden Markov Random Field

Hidden Markov random fields (HMF) are often used as classifiier with atlas-based methods. It can incorporate easily the information coming from the probabilistic atlas as well as the intensities coming from the MRI images. The images are modeled by an undirected graph where the nodes represent the voxels and the edges represent the adjacency between these voxels. The HMF used in this works is similar to the one described in (Scherrer et al., 2009). Y_r and Z_r are considered as random variable field. We denoted $\mathbf{z_r}$ and $\mathbf{y_r}$, a realization of this random variable. A posteriori probability can be expressed in Gibbs form :

$$p(\mathbf{z_r}|\mathbf{y_r},\phi) = W^{-1}exp(-H(\mathbf{z_r}|\mathbf{y_r},\phi)) \qquad (1)$$

With ϕ the model parameters and H a local energy which can be then express as follows:

$$H(\mathbf{z_r}|\mathbf{y_r},\phi) = -\sum_{i\in B_r}[\alpha(v)u(v) + \beta\sum_{q\in\mathcal{N}(v')}z_r(v').z_r(v) + log(p(y_r(v)|z_r(v),\phi))]$$

The information coming from the atlas for the voxel v is weighted with the parameter $\alpha(v)$. The neighborhood information is weighted with the parameter β. $p(y_r(v)|z_r(v),\phi)$ denoted the probability to obtain an intensity if the voxel belong to the region $z_r(v)$. Intensities of each class are modeled by a Gaussian distribution. An initialization is needed and performed with a K-means algorithm with K classes. Only one of these classes is selected to be a *region* class and driven by the atlas ($u(v) = -log(Pr_r(v))$). The other classes are driven by the exterior of the atlas ($u(v) = -log(1 - Pr_r(v))$).

Segmentation is the obtained by finding the Gaussian parameters maximizing the likelihood. This maximization is performed with an Expectation-Maximization algorithm.

3.2 Graph-Cut

In (Boykov et al., 2001), medical images have been processed with a Graph-Cut (GC) method by taking into account a user interaction. GC technics have also been combined and driven by probabilistic atlas (Dangi et al., 2017) or multi-atlas information (Platero et al., 2014).

GC segmentation is also based on a Markov field where the image is described by a graph similarly to HMF. Moreover, two terminal nodes are added representing two classes. A source node describing the *region* and a sink node describing the *background* which are linked to all the other nodes (pixel nodes). GC segmentation is based on finding the segmentation minimizing the energy defined as follows :

$$\mathcal{E}(Z_r) = \mathcal{R}(Z_r) + \mathcal{B}(Z_r) \qquad (2)$$

$\mathcal{R}(Z_r)$ is a region properties term, $\mathcal{B}(Z_r)$ is a boundary properties term and models a surface penalization. $\mathcal{R}(Z_r)$ is computed with the weights present on the edges between the voxels and the terminal nodes. $\mathcal{B}(Z_r)$ is computed with the weights present on the edges between two voxels.

$$\mathcal{B}(Z_r) = \sum_{p,q\in\mathcal{N}} \mathcal{B}_{p,q}.\overline{\delta}(Z_r(p),Z_r(q)) \qquad (3)$$

With $\overline{\delta}(l_1,l_2)$ equal to 1 if l_1 is different to l_2, 0 otherwise. It is commonly depending on the gradient intensities. The weight between a voxel p and a voxel q is fixed to $\mathcal{B}_{p,q} = \frac{exp((Y_r(p)-Y_r(q))^2)}{2\sigma^2}$. σ is the standard deviation of the sub-images B_r.

$$\mathcal{R}(Z_r) = \sum_{v\in Y_r} \mathcal{R}_v(Z_r(v)) \qquad (4)$$

The regional term can model an a priori information about the intensities or the shape but also model an information coming from the user. In this work, the regional term brings the probabilistic atlas information. $\mathcal{R}_v$ is equal to $-log(Pr_r(v))$ for the *region* class and equal to $log(1 - Pr_r(v))$ for the background class. The max-flow min-cut algorithm is performed with the Boykov-Kolmogorov algorithms (boost library) proposed in (Boykov and Kolmogorov, 2004).

3.3 Majority Voting

Majority Voting is one of the easiest and most common way to perform the label fusion step of a multi-atlas segmentation method (Rohlfing et al., 2004; Klein et al., 2005).

Simple Voting Method. After the registration of the available local atlases, the labeled L_r is transformed to the target image space Y_r. The label of each voxel in the sub-image Y_r is then obtained by selecting the label the most frequently provided by the different

label maps. We call this the "simple voting method (SV)" if no weights are used during the merging step. The segmentation of the r is defined as follows :

$$Z_r(v) = \operatorname*{argmax}_{l=\{reg/bg\}} \sum_{a=1}^{N} \delta(L_r^a(v), l) \qquad (5)$$

With $\delta(l_1, l_2)$ equal to 1 if l_1 is equal to l_2, 0 otherwise.

Local Weighted Voting Method. Global (Xabier Artaechevarria, 2008) or local weights (Isgum et al., 2009; Iglesias and Karssemeijer, 2009) have also proposed to merge information coming from the labeled maps. The weights are based on the difference between the registered atlas B_r and the sub-image Y_r. In this works, local weights are applied. The segmentation of the region r is computed as follows :

$$Z_r(v) = \operatorname*{argmax}_{l=reg/bg} \sum_{a=1}^{N} w_a(v)\delta(L_r^a(v), l) \qquad (6)$$

Where $w_a(v)$ is the weight associated to the voxel v in the atlas a. $w_a(v)$ is inversely proportional to the sum square difference between a patch $3 \times 3 \times 3$ around v on Y_r and B_r. In the following, this method is denoted weighted voting method (WV).

3.4 Joint Label Fusion

The Joint Label Fusion method is described in (Wang et al., 2013). It is also a multi-atlas segmentation method with the use of local weights. However these weights are not only based on the similarity between Y_r and the atlases, but take into account the correlation between the atlases. If different atlases seem to bring similar information, the weights are fixed in such way that they act like only one atlas. In practice, the weights are computed in order to minimize the expected label difference between atlases. A correlation matrix $M_v(a, b)$ is computed describing the probability that an atlas a and an atlas b provide the same labeling error at a voxel v. An estimation of this matrix is proposed by comparing the different atlases and the target image to segment. The correlation is computed as follows :

$$M_v(a,b) = [\langle |B_r^a(\mathcal{N}(v)) - Y_r(\mathcal{N}(v))|,$$
$$|B_r^b(\mathcal{N}(v)) - Y_r(\mathcal{N}(v))| \rangle]$$

where $\mathcal{N}(v)$ is a neighborhood around the voxel v. Minimization of the expected label difference leads to define local weights as :

$$\mathbf{w_v} = \frac{M_v^{-1} 1_n}{1_n^t M_v^{-1} 1_n} \qquad (7)$$

with 1_n a unitary vector of size n and w_n a vector of local weights of a voxel v. The final segmentation is achieved in the same manner that the local weighted voting method.

3.5 Convolutional Neural Network

Convolutional Neuron Network (CNN) segmentation have been also applied on medical images especially U-net network. First in 2D (Ronneberger et al., 2015), then in 3D (Çiçek et al., 2016), U-net networks perform an end-to-end segmentation. CNN process is not an atlas-based method as the ones described previously but the network can be train with the same training database than the one used to built the different atlases.

The different couples of training sub-images $\{B_r, L_r\}$ have been used to train several networks. Each of them is built to provide a binary classification for one specific anatomical structure. For each region, the N different couples $\{B_r, L_r\}$ are resized to a multiple of dimension two. A data augmentation is performed by applying a random linear transformation (Random translation, rotation, shear and zoom) to the sub-images. The network is composed of 3 convolutional and 3 deconvolutional layers. Pooling step are performed between each layers. 100 epochs have been used to train each CNN.

Similarly to all the previous methods with local atlases, the sub-image Y_r is extracted and process by the CNN of the region r.

4 COMPARATIVE STUDY

4.1 Experiments

Two experiments have been conducted to compare the different classical methods coupled with the local atlases:

- First experiment (E_1): the different local atlases are positioned inside the test images according to the ground truth. The learned spatial relationships are not used. This situation represent the ideal case where the user position well each bounding box.

- Second experiment (E_2): the efficiency of the different segmentation methods to use the spatial relationships is evaluated. Only the X first regions are positioned with the ground truth. The other bounding boxes are positioned automatically according to the learned spatial relationships. The

segmentation method have to manage the situation when the local atlases are not perfectly positioned inside the whole image.

In the two experiments, the order of segmentation has been fixed. The specification of the machine used to execute the experiments is: Intel(R) Xeon(R), E5, 2.20GHz, 4 cores, 8 Go Ram.

4.2 Image Data Bases

Two image databases have been used during the experiments.

MICCAI. The MICCAI database is a T1 MRI image dataset of the human brain. This dataset has been used during a challenge of multi-atlas segmentation of brain images (Landman et al., 2012). The training part is composed of 15 images and testing part is composed of 20 images. In this work 13 anatomical structures are used. They represent sub-cortical structures that are important for disease diagnostic. An example of the MICCAI data set is illustrated in Figure 2.

SheepBrain. The SheepBrain is a T2 MRI image dataset of ex-vivo adult sheep brains. The images have been acquired by Cyril Poupon (CEA, Neuro-Spin, Saclay) as part of the NeuroGeo [1] project. Six brains were acquired with 7T 50 mT/m MRI with a spatial resolution of 0.3×0.3×0.3 mm. Fifteen anatomical structures have been manually labeled. An example of the SheepBrain dataset is illustrated in Figure 3. As the number of images is low, the experiments have been performed with a one-leave-out process.

4.3 Validation Metrics

The quality of the segmentation is evaluated with the Dice ratio which is a classical metric in medical image segmentation. Dice ratio is computed as follows:

$$Dice = \frac{2VP}{2TP + FP + FN} \qquad (8)$$

where TP is the number of true positive, FP the number of false positives and FN the number of false negative voxels.

4.4 Results

Table 1 describes the Dice ratio obtained for the experiment E_1 on the MICCAI database. WV method provides the best overall results when local atlases are

---

[1] Projet d'intérêt régional CVL N00091714

well positioned. This method seems to be the most robust with satisfactory results on each region (> 82 %). JLF method provides also good segmentations compared to the others, especially for the ventricles. However, this is not the case for the pallidum segmentation which is difficult for JLF method (13.9 % under WV). The 4 other methods have segmentation quality lower than JLF and WV (between 1% and 5% Dice ratio), but always superior to 76 % for all the regions. Figure 4 illustrate qualitative results on an image of a person with Alzheimer's. The segmentation provided by the methods are similar except for ventricles. Large ventricles like in Figure 4(b) are well segmented by JLF method compared to the others. We can also observed that the pallidum is smaller on the JLF segmentation compared to the ground truth.

Table 2 shows the Dice ratio of the E_1 experiment on the SheepBrain database. Contrary to MICCAI database, JLF method achieves better segmentations than all the other methods. The gap between JLF and the others is up to around 3%. WV, SV, HMF and GC methods provide overall result of very similar quality (around 1% between them). The biggest difference between the different methods occurs with the olfactory bulbs which is a very variable region. The registration step is difficult to manage and the classical multi-atlas method or HMF does not succeed to correct wrong registration. For the others anatomical structures, the results are more similar. Contrary to the MICCAI database, the quality of segmentation with CNN is lower than all the other methods. The size of the training database seems to be an important issue. Qualitative results illustrate in the Figure 5 highlight same remarks. Olfactory bulbs segmentation provide by WV, SV and HMF provide very fuzzy borders.

Segmentation quality of the experiment E_2 on the MICCAI database and SheepBrain are shown on Table 3 and Table 4 respectively. With the MICCAI database, only two regions have been well positioned in this experiment ($X = 2$), all the other are positioned with the spatial relationships, leading to an almost automatic segmentation. Contrary to experiments E_1, WV method is very efficient and robust. Overall Dice ratio between E_1 and E_2 only decrease of 1.4 %. Contrary to the JLF segmentation which is not efficient when the positioning is not accurate. The Dice ratio is decreasing by 14.6 % between E_1 and E_2. Small or thin regions like pallidum, caudate nucleus or hippocampus are sometimes completely wrongly segmented, leading to a not accurate utilization of the spatial relationships for the following regions to segment.

With the SheepBrain database, four regions have been well positioned ($X = 4$). Four regions are ne-
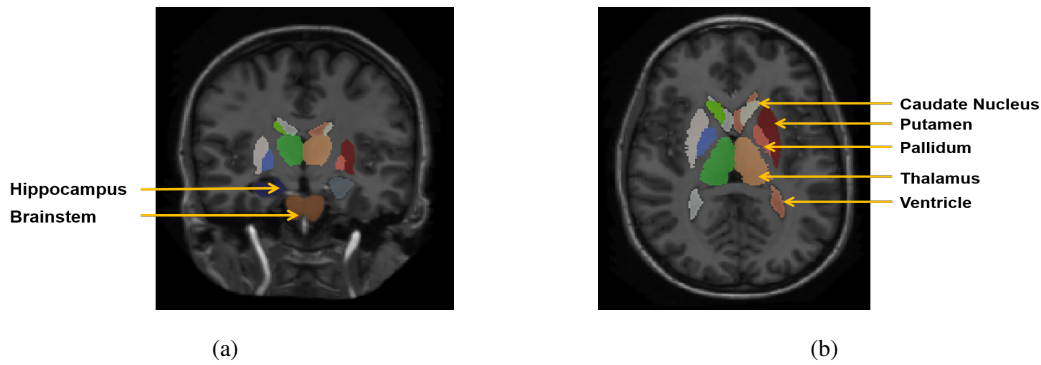
Figure 2: Examples of images and labeled maps associated from the MICCAI database.
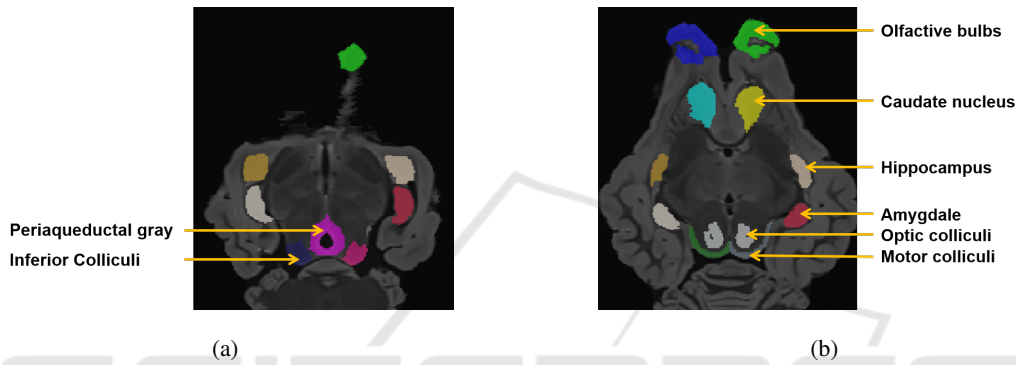
Figure 3: Examples of images and labeled maps associated from the SheepBrain database.

Table 1: Dice ratio (%) of the E_2 experiment on the MICCAI database. Dice ratio of bilateral anatomical structures have been averaged.

Structures	Brainstem	Caud. Nuc.	Hippo.	Vent.	pall.	Puta.	thal.	Average
JLF	93.6	86.1	84.6	90.5	71.0	90.2	90.4	86.1
WV	93.4	86.0	82.0	84.3	84.9	89.9	90.8	86.9
SV	93.3	84.7	80.5	77.3	85.3	90.1	90.6	85.4
HMF	91.5	80.5	78.0	78.8	83.2	88.8	88.1	83.5
GC	91.8	77.0	78.9	76.0	83.3	86.9	89.1	82.6
CNN	90.8	84.7	80.0	78.8	83.1	77.0	89.8	82.9

Table 2: Dice ratio (%) of the E_1 experiment on the SheepBrain database. Dice ratio of bilateral anatomical structures have been averaged.

Structures	Bulb. Olf.	Cau. Nuc.	Peri.	Amyg	Inf. Col.	Opt. Col.	Mot. Col.	Hipp.	Average
JLF	80.0	92.1	85.6	86.1	83.7	82.2	67.0	90.2	83.2
WV	70.9	88.2	86.9	83.6	82.3	80.7	62.5	85.0	79.5
SV	69.5	89.5	88.1	85.1	83.8	82.0	64.6	85.0	80.4
HMF	69.5	86.1	87.3	83.3	83.7	77.6	60.7	88.4	79.1
GC	74.6	87.7	88.9	85.2	84.0	80.2	55.0	87.7	79.8
CNN	56.01	46.8	61.2	62.3	50.9	59.3	54.9	56.5	55.5

cessary because of the small size of the training database and variability of the anatomical structures being more important on the sheep brain images. The overall Dice ratio decreases compared to E_1 for the same reason. However, we can also see that WV still outperform the other segmentation processes. JLF is not

stable and wrong positioning leads directly to wrong segmentations compared to WV.

Table 5 describes the average processing times for the segmentation of the 13 anatomical structures on the MICCAI database. Contrary to the segmentation quality, the computation time is highly different bet-

(a) Ground Truth   (b) JLF

(c) WV   (d) SV

(e) HMF   (f) GC
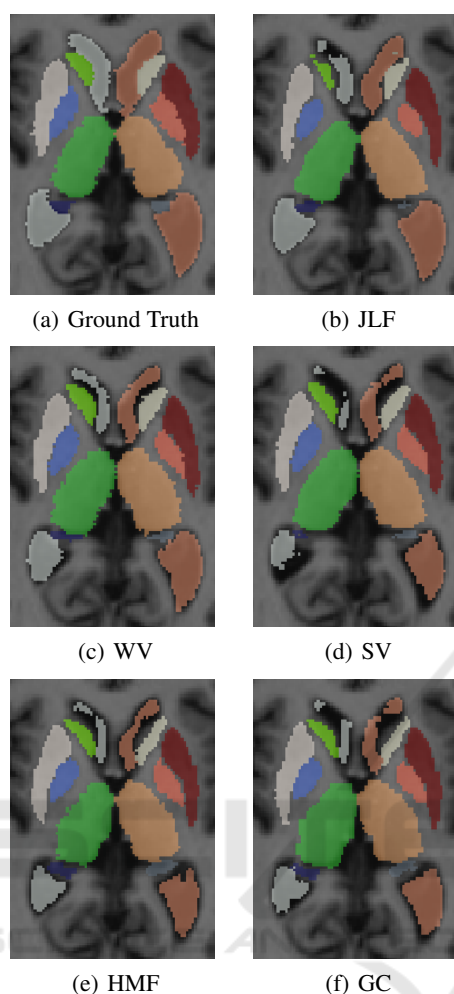
Figure 4: Results of segmentation on the image 1122 for the experiments E_1.

(a) Ground Truth   (b) JLF

(c) WV   (d) SV

(e) HMF   (f) GC

Figure 5: Results of segmentation on a sheep brain image of the SheepBrain database for the experiments E_2.

ween methods. JLF method which provides the best segmentations when local atlases are well positioned is very time consuming compared to all the other methods. In the opposite, only 1 minute is needed by the GC methods to provide the segmentation of 13 regions. This computation time is also dependent of the number of images in the training database. Because of the registration step, multi-atlas based method (SV, WV and JLF) are faster if the size of the training database is small (and vice versa) which is note the case of the methods based on probabilistic atlases (HMF and GC).

5 DISCUSSION

Experiments E_1 and E_2 have been performed without real user interaction. However the method permits the intervention of a user in order to correct the position

of a bounding box. In practice, during an interactive segmentation, the result is close to the one achieve during the experiment E_1. Either the automatic positioning is correct and the user accept it, or the automatic positioning is not correct and the user adjusts the bounding box. In both case, the final position of the bounding box before running the classification step is close to the perfect position. Experiment E_2 described an automatic way to use the system. The first regions are well positioned by the user, then the system ends the segmentation by itself.

The main purpose of this study was to choose the most suitable segmentation method for a local atlas segmentation. The final answer is dependent on the type of utilization that the user wants to perform. During an interactive segmentation, the user needs to have quick visualization of the result which is not pos-

Table 3: Dice ratio (%) of the E_2 experiment on the MICCAI database. Dice ratio of bilateral anatomical structures have been averaged.

Structures	Brainstem	Caud. Nuc.	Hippo.	Vent.	pall.	Puta.	thal.	Average
JLF	78.9	70.5	47.9	75.8	57.7	85.1	89.0	71.5
Weighted Vote	91.4	83.0	80.5	82.5	82.8	89.3	90.7	85.3
Simple Vote	84.43	75.1	56.7	65.1	74.9	85.5	90.4	75.3
HMF	90.1	73.8	69.4	73.0	73.2	85.3	88.1	78.1
GraphCut	75.6	65.3	59.7	62.1	69.1	81.0	88.8	71.3

Table 4: Dice ratio (%) of the E_2 experiment on the SheepBrain database. Dice ratio of bilateral anatomical structures have been averaged.

Structures	Bulb. Olf.	Cau. Nuc.	Peri.	Amyg	Inf. Col.	Opt. Col.	Mot. Col.	Hipp.	Averag
JLF	8.6	92.1	85.6	77.1	52.6	56.0	43.6	75.8	59.8
WV	41.4	88.2	86.9	77.3	64.9	70.1	50.2	80.9	68.9
SV	10.8	89.5	88.1	75.4	46.0	43.4	36.1	66.4	54.9
HMF	24.0	86.1	87.3	82.4	40.1	46.6	37.4	86.8	59.6
GC	5.4	87.7	88.9	79.6	28.8	28.0	13.6	70.5	47.7

Table 5: Average computation time of segmentation of an image in the MICCAI database (E1 experiment).

Method	Computation time
JLF	418 min
WV	22.4 min
SV	10.9 min
HMF	10.1 min
GC	1.1 min
CNN	5 min

sible to achieve with a JLF segmentation method. GC and CNN segmentation provide the labeling of a region in less than 10 seconds which is most suitable for an interactive process. WV, SV and HMF needs between 40 seconds and 2 minutes to obtain the segmentation of a region. Even if these methods seem to provide a better quality than graph-cut segmentation for the MICCAI database, which is even not the case for the SheepBrain database, the gap of quality could not be sufficient to justify their utilization. The time saved by the GC method can be used to apply a manual refinement of the segmentation. However a simple CNN like the one used in this study have shown some limitations when the training database is small.

If an automatic segmentation is desired, the multi-atlas method like JLF and weighted voting are more adapted depending on the time available to perform the segmentation. These methods provide the more precise segmentation and can manage the utilization of the spatial relationships in a better way. In case of wrong positioning, some of the local atlases can be wrongly registered. But the weight which is associated to each atlas in JLF and WV method can limit the importance of some of the local atlases. Depend-

ing on the difficulty of the situation, these methods used in an automatic way can be sufficient.

6 CONCLUSION

In this article, six different atlas-based methods for an interactive and local segmentation of 3D MRI images have been presented and compared. Each classification method have shown to have their own advantages depending on the variability of the position of the anatomical structure and the quality of the initial positioning of the bounding box surrounding the local region to segment. The usage mode of the segmentation tool will justify the final choice. The segmentation of simple regions in an interactive way will lead to the utilization of fast segmentation processes like GC. Difficult regions in an automatic way will lead to more robust segmentation like local weighted majority voting.

ACKNOWLEDGEMENTS

REFERENCES

Ashburner, J. and Friston, K. J. (2005). Unified segmentation. *NeuroImage*, 26(3):839 – 851.

Boykov, Y. and Kolmogorov, V. (2004). An experimental comparison of min-cut/max-flow algorithms for energy minimization in vision. *IEEE Trans. Pattern Anal. Mach. Intell.*, 26(9):1124–1137.

Boykov, Y., Veksler, O., and Zabih, R. (2001). Fast approximate energy minimization via graph cuts. *IEEE Transactions on Pattern Analysis and Machine Intelligence*, 23(11):1222–1239.

Cabezas, M., Oliver, A., Llad, X., Freixenet, J., and Cuadra, M. B. (2011). A review of atlas-based segmentation for magnetic resonance brain images. *Computer Methods and Programs in Biomedicine*, 104(3):e158 – e177.

Çiçek, Ö., Abdulkadir, A., Lienkamp, S. S., Brox, T., and Ronneberger, O. (2016). 3d u-net: Learning dense volumetric segmentation from sparse annotation. In Ourselin, S., Joskowicz, L., Sabuncu, M. R., Unal, G., and Wells, W., editors, *Medical Image Computing and Computer-Assisted Intervention – MICCAI 2016*, pages 424–432, Cham. Springer International Publishing.

Dangi, S., Cahill, N., and Linte, C. A. (2017). Integrating atlas and graph cut methods for left ventricle segmentation from cardiac cine mri. In Mansi, T., McLeod, K., Pop, M., Rhode, K., Sermesant, M., and Young, A., editors, *Statistical Atlases and Computational Models of the Heart. Imaging and Modelling Challenges*, pages 76–86, Cham. Springer International Publishing.

Galisot, G., Brouard, T., Ramel, J., and Chaillou, E. (2017). Image segmentation using local probabilistic atlases coupled with topological information. In *Proceedings of the 12th International Joint Conference on Computer Vision, Imaging and Computer Graphics Theory and Applications (VISIGRAPP 2017) - Volume 4: VISAPP, Porto, Portugal, February 27 - March 1, 2017.*, pages 501–508.

Iglesias, J. E. and Karssemeijer, N. (2009). Robust initial detection of landmarks in film-screen mammograms using multiple ffdm atlases. *IEEE Transactions on Medical Imaging*, 28(11):1815–1824.

Iglesias, J. E. and Sabuncu, M. R. (2015). Multi-atlas segmentation of biomedical images: A survey. *Medical Image Analysis*, 24(1):205 – 219.

Isgum, I., Staring, M., Rutten, A., Prokop, M., Viergever, M. A., and van Ginneken, B. (2009). Multi-atlas-based segmentation with local decision fusionapplication to cardiac and aortic segmentation in ct scans. *IEEE Transactions on Medical Imaging*, 28(7):1000–1010.

Klein, A., Mensh, B., Ghosh, S., Tourville, J., and Hirsch, J. (2005). Mindboggle: Automated brain labeling with multiple atlases. *BMC Medical Imaging*, 5(1):7.

Landman, B. A., Warfield, S. K., Hammers, A., Akhondi-asl, A., Asman, A. J., Ribbens, A., Lucas, B., Avants, B. B., Ledig, C., Ma, D., Rueckert, D., Vandermeulen, D., Maes, F., Holmes, H., Wang, H., Wang, J.,

Doshi, J., Kornegay, J., Hajnal, J. V., Gray, K., Collins, L., Cardoso, M. J., Lythgoe, M., Styner, M., Armand, M., Miller, M., Aljabar, P., Suetens, P., Yushkevich, P. A., Coupe, P., Wolz, R., and Heckemann, R. A. (2012). MICCAI 2012 Workshop on Multi-Atlas Labeling. Technical report.

Nitzsche, B., Frey, S., Collins, L. D., Seeger, J., Lobsien, D., Dreyer, A., Kirsten, H., Stoffel, M. H., Fonov, V. S., and Boltze, J. (2015). A stereotaxic, population-averaged t1w ovine brain atlas including cerebral morphology and tissue volumes. *Frontiers in Neuroanatomy*, 9:69.

Platero, C., Tobar, M. C., Sanguino, J., and Velasco, O. (2014). A new label fusion method using graph cuts: Application to hippocampus segmentation. In Roa Romero, L. M., editor, *XIII Mediterranean Conference on Medical and Biological Engineering and Computing 2013*, pages 174–177, Cham. Springer International Publishing.

Rohlfing, T., Brandt, R., Menzel, R., and Maurer, C. R. (2004). Evaluation of atlas selection strategies for atlas-based image segmentation with application to confocal microscopy images of bee brains. *NeuroImage*, 21(4):1428 – 1442.

Ronneberger, O., Fischer, P., and Brox, T. (2015). U-net: Convolutional networks for biomedical image segmentation. In Navab, N., Hornegger, J., Wells, W. M., and Frangi, A. F., editors, *Medical Image Computing and Computer-Assisted Intervention – MICCAI 2015*, pages 234–241, Cham. Springer International Publishing.

Scherrer, B., Forbes, F., Garbay, C., and Dojat, M. (2009). Distributed local mrf models for tissue and structure brain segmentation. *IEEE Transactions on Medical Imaging*, 28(8):1278–1295.

Shattuck, D. W., Mirza, M., Adisetiyo, V., Hojatkashani, C., Salamon, G., Narr, K. L., Poldrack, R. A., Bilder, R. M., and Toga, A. W. (2008). Construction of a 3d probabilistic atlas of human cortical structures. *NeuroImage*, 39(3):1064 – 1080.

Wang, H., Suh, J. W., Das, S. R., Pluta, J. B., Craige, C., and Yushkevich, P. A. (2013). Multi-atlas segmentation with joint label fusion. *IEEE Transactions on Pattern Analysis and Machine Intelligence*, 35(3):611–623.

Xabier Artaechevarria, Arrate Muoz-Barrutia, C. O.-d.-S. (2008). Efficient classifier generation and weighted voting for atlas-based segmentation: two small steps faster and closer to the combination oracle. *Proc.SPIE*, 6914:6914 – 6914 – 9.